Chemical Science

ROYAL SOCIETY OF CHEMISTRY

EDGE ARTICLE

View Article Online
View Journal | View Issue

Cite this: *Chem. Sci.*, 2021, **12**, 13477

All publication charges for this article have been paid for by the Royal Society of Chemistry

Received 6th June 2021
Accepted 8th September 2021

DOI: 10.1039/d1sc03065e

rsc.li/chemical-science

Real-time imaging of cell-surface proteins with antibody-based fluorogenic probes†

Wenchao Wang,‡[a] Ying Zhang,‡[a] Hong Zhao,‡[a] Xinlei Zhuang,[a] Haoting Wang,[a] Kaifeng He,[ab] Wanting Xu,[a] Yu Kang,[a] Shuqing Chen,[a] Su Zeng[ab] and Linghui Qian *[ab]

Cell-surface proteins, working as key agents in various diseases, are the targets for around 66% of approved human drugs. A general strategy to selectively detect these proteins in a real-time manner is expected to facilitate the development of new drugs and medical diagnoses. Although brilliant successes were attained using small-molecule probes, they could cover a narrow range of targets due to the lack of suitable ligands and some of them suffer from selectivity issues. We report herein an antibody-based fluorogenic probe prepared *via* a two-step chemical modification under physiological conditions, to fulfill the selective recognition and wash-free imaging of membrane proteins, establishing a modular strategy with broad implications for biochemical research and for therapeutics.

Introduction

Due to the importance of cell-surface proteins in maintaining cell homeostasis as well as in dealing with pharmacological intervention,[1–3] methods for selectively detecting the target protein in native environments are in high demand to illustrate its function and evaluate the therapeutic outcomes. Methods relying on genetic engineering to fuse fluorescent proteins directly or to introduce tags like SNAP or PYP proteins,[4,5] peptides,[6,7] or unnatural amino acids[8] followed by the secondary labeling of complementary reporters have been developed. Though valuable, these methods are not feasible to monitor the dynamics of endogenously expressed proteins and may suffer from overexpression issues. Alternatively, probes suitable for the direct visualization of the endogenous protein under live-cell conditions are preferable. Ligands like small-molecule inhibitors,[9,10] protein tags (*e.g.*, cytokine/growth factor),[11] and RNA aptamers[12] have been employed for this purpose. Though powerful, they can only cover a narrow range of targets due to the limitation of available ligands. The specific and high-affinity binding towards antigens, along with mature production techniques, makes antibodies capable to bind virtually any immunogenic target, thus they have been widely used as a modular reagent in both basic research and biomedical applications. Fluorogenic antibody probes, offering antigen-dependent fluorescence responses, could get rid of the time-consuming washing steps and allow real-time imaging. However, the development of such probes is still in its infancy.[13,14] Ueda *et al.* developed antibody fragment-derived "quenchbodies", in which the genetically inserted fluorophore(s) can be quenched by intrinsic tryptophan (Trp) residues and restore upon antigen binding.[15,16] Later, Hohsaka's group utilized selective N-terminal alkylation to simplify the fluorophore labeling.[17] It is to be noted that such a fluorescence change is highly dependent on the amount and localization of Trp residues on the antibody, and thus efforts are still needed to develop a "universal" strategy for easy conversion of commercially available antibodies into fluorogenic probes.

Antibodies have a Y-shaped structure, where the N-termini of heavy (H) and light (L) chains come together to form two identical antigen-binding sites at the tips. We envisioned that two fluorophores situated on the H/L chains of the same "Y" tip are prone to form dye–dye interaction, and it is likely to be disrupted upon antigen binding. Herein we focus on dyes that undergo self-quenching in aqueous media through H-type dimerization *via* π–π stacking,[9,18–21] while getting restored upon disaggregation. In addition, improved signal-to-background contrast would be achieved if the dye is environment-sensitive, due to its proximity to the hydrophobic plasma membrane upon interacting with cell-surface targets. To fulfill the above requirements, sulforhodamine B (SRB) was chosen according to its optimal photophysical properties and the dimerization-induced self-quenching potency.[19] Meanwhile, 2-pyridinecarboxaldehyde (2PCA) was used for N-terminal

[a]*Institute of Drug Metabolism and Pharmaceutical Analysis, Zhejiang Province Key Laboratory of Anti-Cancer Drug Research, College of Pharmaceutical Sciences, Cancer Center, Zhejiang University, Hangzhou 310058, China. E-mail: lhqian@zju.edu.cn*

[b]*Hangzhou Institute of Innovative Medicine, Zhejiang University, Hangzhou 310018, China*

† Electronic supplementary information (ESI) available: Experimental procedures, characterization of all new compounds, HRMS and NMR spectra, and supplementary figures. See DOI: 10.1039/d1sc03065e

‡ These authors contributed equally.

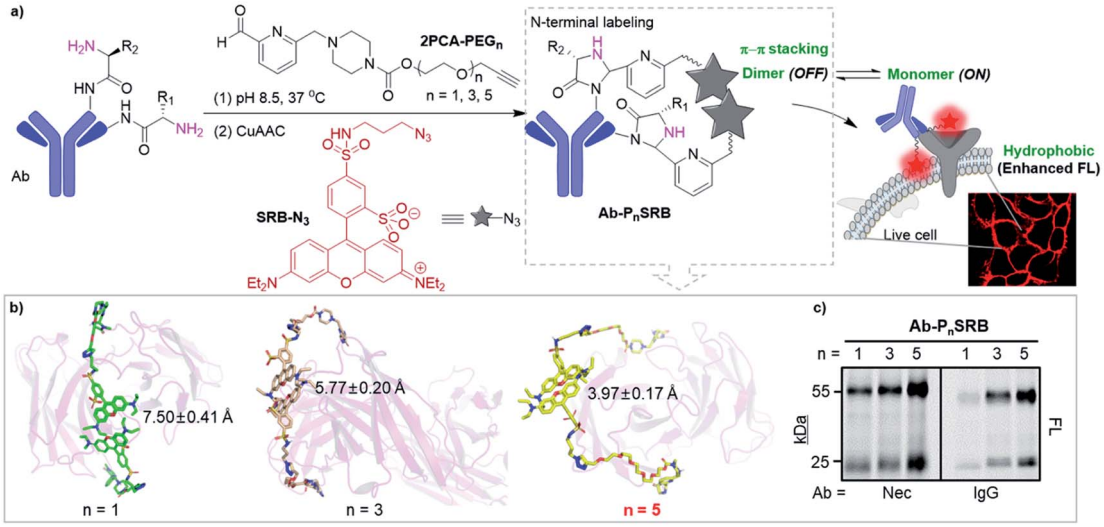

Fig. 1 Strategy of antibody-based fluorogenic probes (**Ab-P$_n$SRB**, *n* indicates the PEG length). (a) Schematic illustration of cell-surface protein imaging with antibody-based probes prepared by two-step labeling (details are shown in Scheme S3†). (b) The representative conformations of **2PCA–PEG$_n$/SRB-N$_3$** (**P$_n$SRB** in short) labeled necitumumab (Nec) at the stable trajectories. Average distances and SDs between the centroid of the xanthene of two SRBs were calculated. (c) Labeling efficiency of **2PCA–PEG$_n$/SRB-N$_3$** towards antibodies (*i.e.*, necitumumab and human IgG), which was visualized by in-gel fluorescent scanning (FL).

modification of antibodies under mild conditions.[22,23] To realize efficient quenching and antigen-responsive "switch on" of SRB, the linker between SRB and 2PCA is critical. A two-step labeling strategy is thus proposed, where 2PCA coupled with different lengths of PEG linkers along with a terminal alkyne (**2PCA–PEG$_n$**, Scheme S1†) was first used to tag the antibody. Then SRB containing an azide group (**SRB-N$_3$**, Scheme S2†) was conjugated through click chemistry to form the antibody-based fluorogenic probe, **Ab-P$_n$SRB** (Fig. 1a and Scheme S3†). The two-step strategy can reduce the burden on chemical synthesis as well as ensuring the labeling efficiency since PEG-containing 2PCA derivatives should have improved water solubility even at high concentrations. As a proof of concept, the epidermal growth factor receptor (EGFR) and anti-EGFR therapeutic antibodies, necitumumab (Nec) and cetuximab (Cet), were studied here. Live-cell imaging showed that after chemical labeling, both antibodies showed EGFR-dependent fluorescence, exhibiting the potential of this strategy for detecting cell-surface proteins with commercially available antibodies.

Results and discussion

Initially, molecular dynamics (MD) simulation was carried out to delineate the distance between two SRBs when situated at the N-termini of H/L chains on the same tip of necitumumab and cetuximab (Fig. S1†). As shown in Fig. 1b and S2,† when $n = 5$, SRBs in both necitumumab and cetuximab are close to each other with a distance between 3.7 and 4.0 Å, ideal for face-to-face π–π stacking.[24–26] Therefore the resulting **Ab-P$_5$SRB** is expected to have the desired quenching effect in aqueous solution. In addition, the labeling experiments (Scheme S3†) exhibited that, when $n = 5$, the dye-to-protein ratio was the highest among the three (Fig. 1c and S3a†), estimated to be

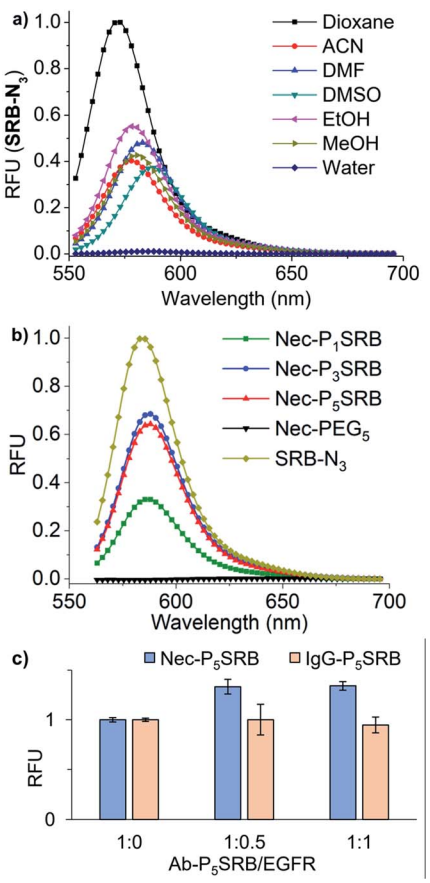

Fig. 2 Photophysical properties of **SRB-N$_3$** and the resulting **Ab-P$_n$SRB** probes. (a) Fluorescence spectra of **SRB-N$_3$** (5 μM) in different solvents (λ_{ex} = 530 nm). (b) Fluorescence spectra of **Nec-P$_n$SRB** (100 nM) and **SRB-N$_3$** (20 nM) in H_2O (λ_{ex} = 530 nm). (c) Fluorescence response of **Nec-P$_5$SRB/IgG-P$_5$SRB** (20 nM) in the presence of recombinant EGFR at different ratios (λ_{ex} = 560 nm and λ_{em} = 590 nm).

around 75% (Table S1†). It is likely due to the better water solubility of **2PCA–PEG$_5$** than the other two, when a high concentration of the probe (10 mM) was used to promote the labeling efficiency (data not shown).[22,23] Moreover, the labeling ratio of **2PCA–PEG$_5$/SRB-N$_3$** (**P$_n$SRB** in short) towards different antibodies (*i.e.*, IgG, Nec, and Cet) was similar (Fig. S3b; the amino acid sequences of the Fab fragments of Nec and Cet are shown in the ESI†), promising in view of universality.

After confirming that the antibody retained the ability to bind its antigen after modification with **P$_5$SRB** (Fig. S4†), we evaluated the photophysical properties *in vitro*. SRB was reported to form a quenched dimer in water when closely connected, and the π–π effect was disrupted in MeOH.[19] As shown in the absorption spectra (Fig. S5a†), a blue shifted band (530 nm) appeared in water at higher concentrations, indicating the enhancement of dimeric H-aggregation.[19] Along with that, an increased fluorescence discrepancy between water and MeOH as the concentration of **SRB-N$_3$** grew was observed (Fig. S5b†), likely due to the increment of SRB dimerization at higher concentrations in water. Upon the addition of MeOH to water, **SRB-N$_3$** showed fluorescence recovery similar to the classical solvatochromic fluorophore, 4-sulfamonyl-7-aminobenzoxadiazole (SBD)[27] (Fig. S6a†). And stronger emission was seen in all tested organic solvents than in water for **SRB-N$_3$** and SBD (Fig. 2a and S6b†), but not for the control, rhodamine B (TER-N$_3$; structure shown in Scheme S3†). Thus **SRB-N$_3$** is regarded as environment-sensitive as well. After being conjugated to the N-termini of antibodies, the resulting **Ab-P$_n$SRB** (100 nM) showed much weaker fluorescence than the free **SRB-N$_3$** (20 nM, Fig. 2b), suggesting that obvious fluorescence quenching occurred. Since in the absorption spectra (Fig. S7a†), a higher ratio of $A_{530\ nm}/A_{560\ nm}$ was seen from **Nec-P$_n$SRB** in water than that from **SRB-N$_3$** in MeOH, the quenching is partially due to the dimeric H-aggregation. Meanwhile the background signal was still seen in comparison with the unlabeled Nec, largely due to the relatively low labeling ratio of Nec by **2PCA–PEG$_n$**. If all of the four N-terminal amines on antibodies were labeled by SRB, dimerization would occur between the H and L chain on the same tip for stronger quenching. Nevertheless, **Nec-P$_5$SRB** showed no stronger fluorescence than **Nec-P$_3$SRB**, even though its labeling ratio is much higher, suggesting that the quenching efficiency in **Nec-P$_5$SRB** was much stronger, consistent with the MD simulation results. In contrast, the conjugation of TER-N$_3$ to the N-termini of the

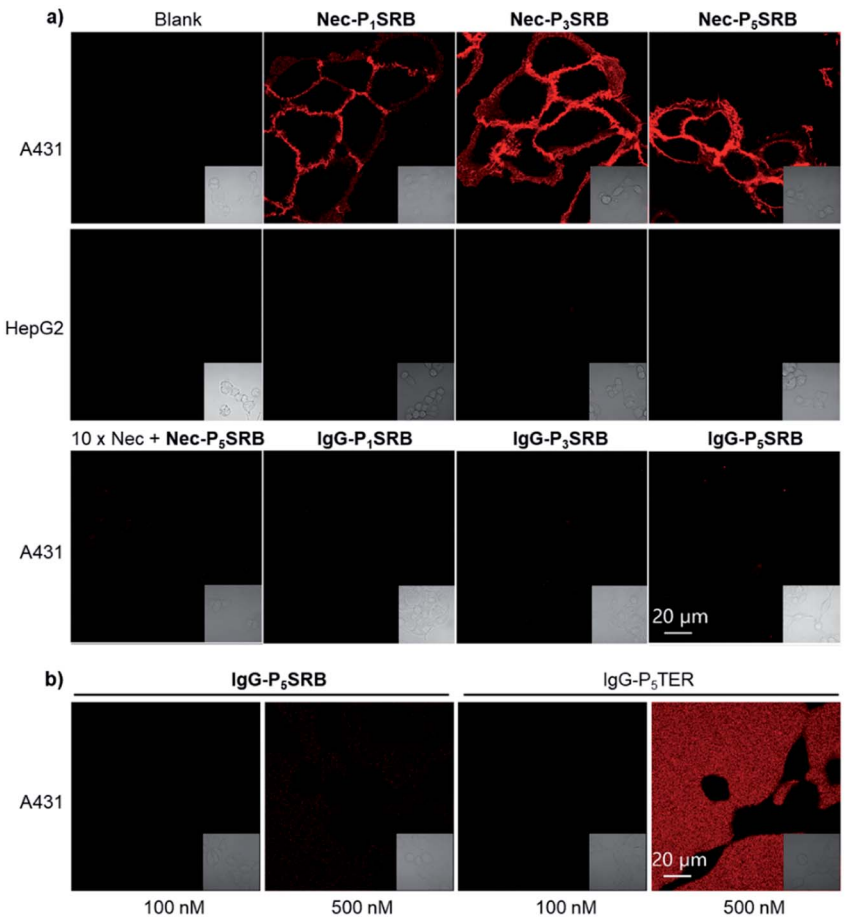

Fig. 3 Live-cell imaging by using **Ab-P$_n$SRB** (λ_{ex} = 561 nm and λ_{em} = 581–639 nm). (a) Cellular performance of **Nec-P$_n$SRB** (100 nM) in both EGFR-positive (A431) and EGFR-negative (HepG2) cells. 10× Nec means that cells were pretreated with 1 μM of necitumumab for 0.5 h before the addition of **Nec-P$_5$SRB**. Control probes **IgG-P$_n$SRB** (100 nM) were studied in parallel. (b) Comparison of the background signal from **IgG-P$_5$SRB** and that from IgG-P$_5$TER ("always-on" probe) in A431 cells without washing.

antibody did not show an obvious fluorescence decrease (Fig. S7b†), confirming that the efficient quenching effect was mainly due to the photophysical properties of **SRB-N$_3$**. Upon addition of recombinant EGFR, the fluorescence intensity of **Nec-P$_5$SRB** increased within 30 min (Fig. 2c). In contrast, there was no "off-on" change from the negative control, **IgG-P$_5$SRB**. *In vitro* experiments also showed that the antigen-response fluorescence enhancement was moderate and got saturated in the presence of less than 1 equivalent of EGFR, again, possibly attributed to the low labeling ratio of SRB.

Afterwards, we turned our attention to live-cell imaging by using **Nec-P$_n$SRB**, to check the "synergetic" switch-on potency by the hydrophobic plasma membrane. Initially, in concentration-dependent experiments, **Nec-P$_5$SRB** showed detectable red fluorescence on the surface of the EGFR-positive cancer cell A431 even at a concentration as low as 20 nM (Fig. S8a†). As the probe concentration increased, all three probes showed brilliant emission, especially at a concentration of 100 nM (Fig. 3a, top), and thus we used this concentration for the subsequent live-cell imaging experiments if not specified. It is to be noted that the signal-to-background contrast of **Nec-P$_1$SRB** was much lower than that of **Nec-P$_5$SRB**, likely due to its weaker quenching efficiency as shown in previous *in vitro* results (Fig. S8b†). Meanwhile, the fluorescence signal can be fully eliminated when competed by excess Nec, and control groups including the low EGFR expression cell (*i.e.*, HepG2) or using **IgG-P$_n$SRB** (human IgG, without a specific binding target) showed no fluorescence signal (Fig. 3a, middle and bottom). These results together confirmed the EGFR-response fluorescence of **Nec-P$_5$SRB** in living cells. It is worth noting that our **Ab-P$_n$SRB** was designed to be quenched without binding to cell-surface EGFR. To check the background of the probe under a microscope, **IgG-P$_5$SRB** and IgG-P$_5$TER (prepared as shown in Scheme S3†) were incubated with A431, respectively, for no-wash imaging. Here TER was used

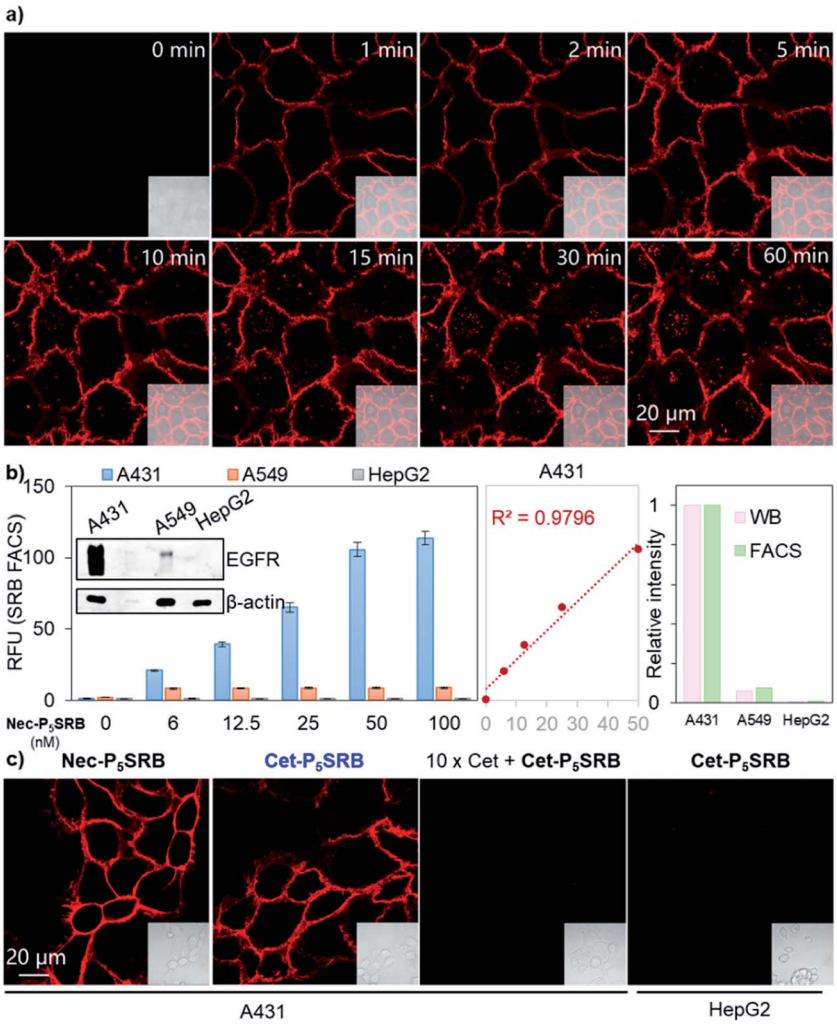

Fig. 4 Applications of **Ab-P$_5$SRB** for detecting endogenous EGFR in living cells. (a) Real-time imaging of A431 cells upon addition of **Nec-P$_5$SRB** (100 nM). (b) FACS of **Nec-P$_5$SRB** towards A431/A549/HepG2 (left). Western blotting (WB) analysis of EGFR in A431/A549/HepG2 (inset). Linear correlation analysis between the average fluorescence in A431 and probe's concentration (middle). Relative intensity readings extracted from WB (pink) *versus* those from FACS (green) (right). (c) No-wash imaging of A431/HepG2 cells obtained by using **Cet-P$_5$SRB** (100 nM). 10 × Cet in the third panel means that cells were pretreated with 1 μM of cetuximab for 0.5 h before the addition of **Cet-P$_5$SRB**. λ_{ex} = 561 nm and λ_{em} = 581–639 nm for all cell imaging.

as a representative "always-on" reporter for comparison. As shown in Fig. 3b, a negligible background was seen for both probes at 100 nM, while at 500 nM, strong red background was observed in IgG-P_5TER treated cells. In sharp contrast, the background of the image using **IgG-P_5SRB** remained almost dark, where the self-quenching H-aggregation and environmental sensitivity may dominate the non-fluorescent status of SRB in aqueous solution.

With a low-background and selective fluorogenic probe in hand, real-time imaging was carried out using **Nec-P_5SRB** (Fig. 4a and S9†). Brilliant fluorescence was detected on the cell membrane immediately after the addition of the probe. Intracellular fluorescence was detected after 5 min in some cells and became obvious in most cells after 30 min, as caused by the internalization of the antibody–EGFR complex.[28,29] Taken together, we concluded that **Nec-P_5SRB** was indeed suitable for real-time imaging of endogenous EGFR in live mammalian cells. To take one step further, endogenous EGFR expression levels in different cell lines were quantitatively analyzed by using **Nec-P_5SRB** with FACS. Fig. 4b shows that the average fluorescence intensity in A31 cells increased linearly with the probe concentration in the range of 0 to 50 nM and got saturated at 100 nM. In A549 cells, the saturation was observed at much lower concentrations of **Nec-P_5SRB**, while the signal remained very weak in HepG2 cells at all concentrations. Interestingly, the fluorescence readings obtained at the saturation concentration (*i.e.*, 100 nM) from FACS showed consistent EGFR protein levels with the results obtained from WB analysis. These results demonstrated that our probe can not only indicate the dynamic localization of endogenous EGFR, but also be used for quantitative analysis.

To test the robustness and practicality of this strategy for other antibodies with different amino acid sequences, **2PCA–PEG_5** labeling followed by **SRB-N_3** click ligation was applied to another EGFR-targeting antibody, cetuximab, under the same conditions. Identical cellular performance was seen between **Cet-P_5SRB** and **Nec-P_5SRB** (Fig. 4c), with minimal effect on the binding affinity of cetuximab (Fig. S10†), suggesting that this strategy has high potential as a universal method to create antibody-based fluorogenic probes towards cell-surface proteins.

Conclusions

In conclusion, we have developed an easy-operation two-step labeling strategy to create fluorogenic antibody-based probes for real-time imaging of cell surface proteins. Thanks to antibody's capability of binding to virtually any immunogenic target with exquisite specificity and high affinity, the resulting probe is highly selective and this method is promising to be applied for detecting any cell-surface protein with commercially available antibodies. Current efforts are focused on the development of probes with other colors as well as figuring out the chemistry for better labeling efficiency at N-termini.

Data availability

Supporting data for this article is presented in the ESI.†

Author contributions

L. Q. designed the project. W. W., Y. Z., X. Z., H. W., K. H., and W. X. carried out the experiments; H. Z. and Y. K. carried out the MD simulation and analysis. W. W., Y. Z. and H. Z. contributed equally. S. C. guided the biological experiments and the writing. L. Q. and S. Z. directed the project and wrote the manuscript. All authors commented on the manuscript.

Conflicts of interest

There are no conflicts to declare.

Acknowledgements

We are grateful for the financial support from the National Natural Science Foundation of China (81903574) and the Fundamental Research Funds for the Central Universities (2019QNA7046, 2020QNA7001). We also acknowledge generous financial support from Zhejiang University. We thank Ms Haihong Hu and Ms Li Ma for managing instruments and helping with experiments. We also thank Jianyang Pan (Research and Service Center, College of Pharmaceutical Sciences, Zhejiang University) for performing NMR spectrometry.

Notes and references

1 L. Kuhlmann, E. Cummins, I. Samudio and T. Kislinger, *Expert Rev. Proteomics*, 2018, **15**, 259–275.
2 D. Bausch-Fluck, U. Goldmann, S. Müller, M. van Oostrum, M. Müller, O. T. Schubert and B. Wollscheid, *Proc. Natl. Acad. Sci. U. S. A.*, 2018, **115**, E10988–E10997.
3 K. K. Leung, G. M. Wilson, L. L. Kirkemo, N. M. Riley, J. J. Coon and J. A. Wells, *Proc. Natl. Acad. Sci. U. S. A.*, 2020, **117**, 7764–7775.
4 A. Keppler, S. Gendreizig, T. Gronemeyer, H. Pick, H. Vogel and K. Johnsson, *Nat. Biotechnol.*, 2003, **21**, 86–89.
5 J. Gao, Y. Hori, M. Nishiura, M. Bordy, J. Hasserodt and K. Kikuchi, *Chem. Lett.*, 2020, **49**, 232–235.
6 J. Lotze, U. Reinhardt, O. Seitz and A. G. Beck-Sickinger, *Mol. BioSyst.*, 2016, **12**, 1731–1745.
7 G. C. Gavins, K. Gröger, M. D. Bartoschek, P. Wolf, A. G. Beck-Sickinger, S. Bultmann and O. Seitz, *Nat. Chem.*, 2021, **13**, 15–23.
8 A. I. König, R. Sorkin, A. Alon, D. Nachmias, K. Dhara, G. Brand, O. Yifrach, E. Arbely, Y. Roichman and N. Elia, *Nanoscale*, 2020, **12**, 3236–3248.
9 Y. Jiao, J. Yin, H. He, X. Peng, Q. Gao and C. Duan, *J. Am. Chem. Soc.*, 2018, **140**, 5882–5885.
10 Q. Wu, Y. Jing, T. Zhao, J. Gao, M. Cai, H. Xu, Y. Liu, F. Liang, J. Chen and H. Wang, *Nanoscale*, 2020, **12**, 21591–21598.
11 Y. Takaoka, S. Uchinomiya, D. Kobayashi, M. Endo, T. Hayashi, Y. Fukuyama, H. Hayasaka, M. Miyasaka, T. Ueda, I. Shimada and I. Hamachi, *Chem*, 2018, **4**, 1451–1464.

12 X. Tan, T. P. Constantin, K. L. Sloane, A. S. Waggoner, M. P. Bruchez and B. A. Armitage, *J. Am. Chem. Soc.*, 2017, **139**, 9001–9009.
13 T. Hayashi, Y. Yasueda, T. Tamura, Y. Takaoka and I. Hamachi, *J. Am. Chem. Soc.*, 2015, **137**, 5372–5380.
14 K. He, S. Zeng and L. Qian, *J. Pharm. Anal.*, 2020, **10**, 397–413.
15 R. Abe, H. Ohashi, I. Iijima, M. Ihara, H. Takagi, T. Hohsaka and H. Ueda, *J. Am. Chem. Soc.*, 2011, **133**, 17386–17394.
16 H.-J. Jeong, T. Kawamura, M. Iida, Y. Kawahigashi, M. Takigawa, Y. Ohmuro-Matsuyama, C.-I. Chung, J. Dong, M. Kondoh and H. Ueda, *Anal. Chem.*, 2017, **89**, 10783–10789.
17 K. Fukunaga, T. Watanabe, D. Novitasari, H. Ohashi, R. Abe and T. Hohsaka, *Chem. Commun.*, 2018, **54**, 12734–12737.
18 I. A. Karpenko, M. Collot, L. Richert, C. Valencia, P. Villa, Y. Mély, M. Hibert, D. Bonnet and A. S. Klymchenko, *J. Am. Chem. Soc.*, 2015, **137**, 405–412.
19 F. Bouhedda, K. T. Fam, M. Collot, A. Autour, S. Marzi, A. Klymchenko and M. Ryckelynck, *Nat. Chem. Biol.*, 2020, **16**, 69–76.
20 L. Esteoulle, F. Daubeuf, M. Collot, S. Riché, T. Durroux, D. Brasse, P. Marchand, I. A. Karpenko, A. S. Klymchenko and D. Bonnet, *Chem. Sci.*, 2020, **11**, 6824–6829.
21 K. T. Fam, M. Collot and A. S. Klymchenko, *Chem. Sci.*, 2020, **11**, 8240–8248.
22 J. I. MacDonald, H. K. Munch, T. Moore and M. B. Francis, *Nat. Chem. Biol.*, 2015, **11**, 326–331.
23 D.-Z. Li, B.-N. Han, R. Wei, G.-Y. Yao, Z. Chen, J. Liu, T. C. W. Poon, W. Su, Z. Zhu, D. S. Dimitrov and Q. Zhao, *mAbs*, 2018, **10**, 712–719.
24 R. Zhao and R.-Q. Zhang, *Phys. Chem. Chem. Phys.*, 2016, **18**, 25452–25457.
25 L. He, P. Wang, L. He, Z. Qu, J. Luo, B. Peng, X. Tang and Y. Pei, *RSC Adv.*, 2018, **8**, 11134–11144.
26 K. Carter-Fenk and J. M. Herbert, *Phys. Chem. Chem. Phys.*, 2020, **22**, 24870–24886.
27 Y.-D. Zhuang, P. Y. Chiang, C.-W. Wang and K.-T. Tan, *Angew. Chem., Int. Ed.*, 2013, **52**, 8124–8128.
28 J. B. Spangler, J. R. Neil, S. Abramovitch, Y. Yarden, F. M. White, D. A. Lauffenburger and K. D. Wittrup, *Proc. Natl. Acad. Sci. U. S. A.*, 2010, **107**, 13252–13257.
29 X. Shi, C. Y. Y. Yu, H. Su, R. T. K. Kwok, M. Jiang, Z. He, J. W. Y. Lam and B. Z. Tang, *Chem. Sci.*, 2017, **8**, 7014–7024.